IEEE Access
Multidisciplinary ⋮ Rapid Review ⋮ Open Access Journal

Received 25 March 2023, accepted 4 May 2023, date of publication 10 May 2023, date of current version 18 May 2023.

Digital Object Identifier 10.1109/ACCESS.2023.3275101

APPLIED RESEARCH

Implementation of a High-Speed Multichannel Data Acquisition System for Magnetic Diagnostics and Plasma Centroid Position Control in ISTTOK

DOMÉNICA CORONA[1,2], ADRIANO MELE[3], NUNO CRUZ[1,4], HUGO ALVES[1], BERNARDO B. CARVALHO[1], HUMBERTO FIGUEIREDO[1], AND HORACIO FERNANDES[1]

[1]Instituto de Plasmas e Fusão Nuclear, Universidade de Lisboa, 1049-001 Lisboa, Portugal
[2]Princeton Plasma Physics Laboratory, Princeton, NJ 08540, USA
[3]Dipartimento di Economia, Ingegneria, Società e Impresa, Università degli Studi della Tuscia, Largo dell'Università—Campus Riello, 01100 Viterbo, Italy
[4]Consorzio RFX, 35127 Padua, Italy

Corresponding authors: Doménica Corona (lcoronar@pppl.gov) and Adriano Mele (adriano.mele@unitus.it)

This work was supported in part by the Fundaçao para a Ciência e a Tecnologia (FCT) under Grant PD/BD/114306/2016; in part by the Framework of the Advanced Program in Plasma Science and Engineering (APPLAuSE) sponsored by FCT under Grant PD/00505/2012; and in part by the Instituto de Plasmas e Fusão Nuclear (IPFN) through FCT under Project UID/FIS/50010/2019, Project UIDB/50010/2020, and Project UIDP/50010/2020. The work of Doménica Corona was supported by the Italian Ministry for University and Research (MUR) under the Young Independent Research Group (YIRG) Project SOLEMIO under Grant 737/2021. The work of Adriano Mele was supported in part by the Italian Ministry for University and Research (MUR) under the European Social Fund Recovery Assistance for Cohesion and the Territories of Europe (REACT EU)—PON Ricerca e Innovazione (2014–2020) under Grant 1062/2021; and in part by MUR under YIRG Project SOLEMIO under Grant 737/2021. The work of Nuno Cruz was supported by the Framework of the EUROfusion Consortium funded by the European Union via the Euratom Research and Training Programme through EUROfusion under Grant 101052200.

ABSTRACT In tokamak and other fusion devices, magnetic control is the main tool that allows to regulate the plasma current, position and shape; it is in charge of actuating the desired plasma current waveform, steering the plasma position to a given set point and maintain the plasma shape close to a prescribed plasma equilibrium. This work describes the application of several physics concepts and computational tools in order to obtain a novel optimal controller for the plasma centroid position, which has been implemented and tested in the real-time plasma control system at the ISTTOK tokamak. A key point for the development of the new control system was the installation of a recently upgraded hardware, that numerically integrates in real-time the magnetic probes signals.

INDEX TERMS Real-time control, plasma current, plasma current centroid position, magnetic probe, poloidal field coils, numerical integration.

I. INTRODUCTION

Tokamaks [1] are experimental devices used in nuclear fusion research, in which a hot plasma (from tens to hundreds of millions of degrees) is confined in a toroidal (i.e. doughnut-shaped) vacuum chamber by strong magnetic fields. Currently, tokamaks are considered the most promising concept to achieve energy production through nuclear fusion reactions.

In tokamaks, a number of dedicated control systems are used to regulate and maintain the performance of the plasma, and to protect the device itself. Such systems are crucial to achieve stable and sustained fusion reactions, and are in charge of controlling a wide range of plasma parameters [2]. Among these systems, plasma magnetic control [3], [4], [5] is devoted to actuating the currents in the so-called *Poloidal Field Coils* (PFC), i.e. a set of windings (often made of superconductive materials in modern reactors) that are used to generate the magnetic fields needed to confine the plasma and regulate quantities such as the total plasma current, the current centroid position and the plasma shape (defined on the basis of the magnetic field topology as the last closed magnetic flux surface which is completely inside the vacuum chamber - see for example [6]). In addition, this system is also used to stabilize the $n = 0$ plasma vertical instability [7], [8].

The practical implementation of any of the control systems of a tokamak, including the magnetic one, involves a combination of reliable sensors, fast actuators and specific control

The associate editor coordinating the review of this manuscript and approving it for publication was Dong Shen.

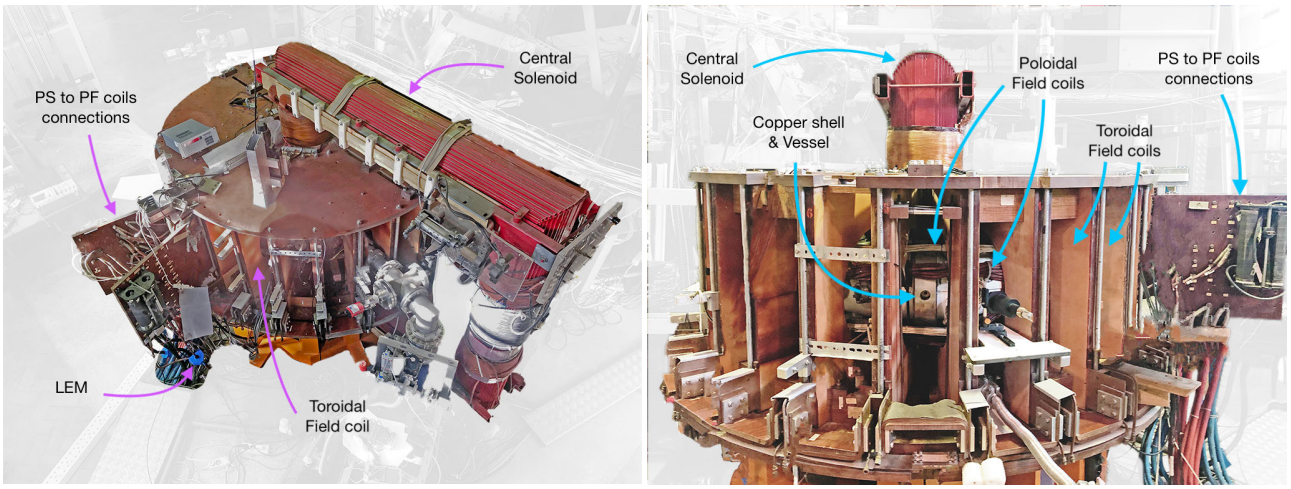

FIGURE 1. Left: ISTTOK top view, the main elements are indicated with magenta lines. Right: frontal view, the main components considered in this article are indicated with blue lines.

algorithms. Specifically, since directly sensing fusion plasmas is impractical due to their extreme temperatures and the potential for plasma contamination, specialized techniques are frequently employed to reconstruct the desired quantities based on indirect measurements [9], [10], [11].

In this paper, we discuss the implementation of the diagnostic and control system for the plasma current centroid position in the ISTTOK tokamak [12]. ISTTOK is a circular cross-section research tokamak operated at the Instituto Superior Técnico, Lisbon. It has a major radius of 46 cm and minor radius of 8.5 cm, with a nominal toroidal field of $0.3-0.6$ T which can reach a maximum of 2.8 T. ISTTOK has an iron-core transformer and a graphite limiter, and it has the peculiarity of being capable of operating in both Direct and Alternate Current, with a maximum plasma current of 7 kA.

The real-time integration of diagnostic signals enabled a reliable reconstruction of the plasma current centroid position. The availability of these real-time data for the plasma position facilitated the implementation of novel and more accurate control techniques.

The rest of the paper is structured as follows. The ISTTOK magnetic configuration is first introduced in Section II, followed by the hardware implementations in Section III, and the real-time software integration in Section IV. Section V presents the real-time plasma position control system, while Section VI discusses the experimental results obtained with such system. Some conclusions are eventually drawn in Section VII.

II. ISTTOK TOKAMAK

Many ISTTOK components, such as the vacuum systems, the PFCs, and the power supply for the toroidal magnetic coils, as well as its diagnostics and control&data acquisition system, were locally designed and built at the Instituto Superior Técnico, Lisbon. Figure 1 shows a top and a frontal view of the ISTTOK tokamak. The main elements are indicated in the figure.

A. ISTTOK AC PLASMA CURRENT

ISTTOK main characteristic is that, thanks to the flexibility of the power supplies and their relatively low electrical time constants, it is possible to perform AC discharges which allow the fast reversal of the plasma current while maintaining a finite plasma density between consecutive flat tops [13]. During the AC discharges, the toroidal field B_ϕ is kept unchanged, but the plasma inversion result in a reversal in the generated poloidal which requires in turn a change of sign of the equilibrium vertical field required to achieve the desired toroidal force balance. ISTTOK's dwell time in between two cycles is adjustable, but it is normally chosen equal to ~ 1 *ms*.

B. DIAGNOSTICS AND ACTUATORS

ISTTOK integrates a set of different diagnostics to retrieve important plasma parameters, including Langmuir probes, interferometry, tomography and magnetic probes [14]. In particular, ISTTOK has a set of 12 poloidally distributed magnetic field probes (*Mirnov coils*), as shown in figure 2. Three-dimensional computer models of the pick-up coils and of their graphite mounting boxes are shown in figure 3.

Figure 4a shows the vessel side port, where the magnetic probes are placed and the probes acquisition cables, along with some of the PFCs cables in orange and white. Magnetic probes are capable of picking up the induced voltage due to Faraday's law

$$\varepsilon = -N\frac{d\Phi_P}{dt},$$

where Φ_P is the total poloidal magnetic flux generated by the plasma, the PF-Coils and the passive elements and enclosed by the probe cross-section, and N is the number of turns of the probe coil. The relatively small cross-section of the

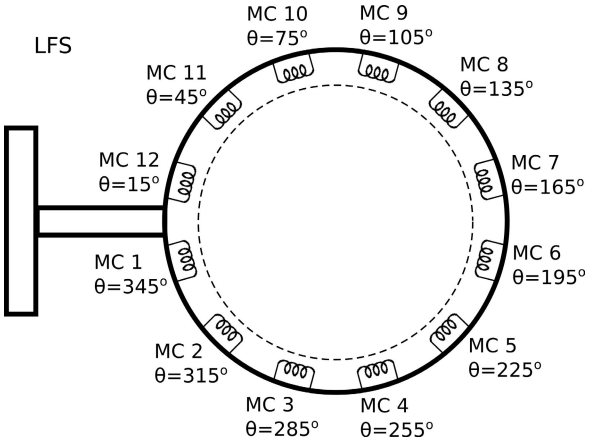

FIGURE 2. Set of 12 poloidal magnetic field probes for the reconstruction of the plasma centroid position at ISTTOK, with the corresponding poloidal angles. The Low-Field Side is indicated as LFS.

(a) 3D model of a single ISTTOK magnetic probe coil.

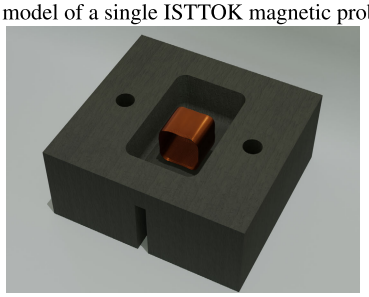

(b) 3D model of one graphite box which conforms the plasma facing limiter and contains a magnetic probe inside. Each probe is capsuled inside a graphite box, cut horizontally to avoid eddy-currents.

FIGURE 3. ISTTOK magnetic probes.

Mirnov coils allows to assume that the magnetic field remains approximately constant over the probe volume.

C. POLOIDAL FIELD COILS

ISTTOK's Poloidal Field (PF) coils are connected to three independently feedback-controlled power supplies, for the purpose of generating plasma current and of controlling the plasma current centroid's vertical and horizontal position. Figure 6 depicts, on the right side of the iron core, an old central solenoid which used to be responsible for plasma current generation; this element is currently disconnected, and has been replaced by another one on the limb of the transformer. The primary PFCs, in white color, generate Ohmic heating for the creation of plasma current and an additional vertical field. The vertical PFCs are shown in yellow, while the horizontal PFCs are in green. These groups of coils are controlled by different control algorithms in order to follow a centroid position set-point [15]. The poloidal field geometries generated by these three independent circuits are shown in figure 5.

Figures 4a and 4b show the cables from the PFCs arranged in sets of orange (Vertical and Horizontal PFCs) and white cables (Ohmic Heating coils).

From the pictures in figure 4 it is clear that due to strong space constraints and a vacuum vessel with a multitude of diagnostics ports, especially the vertical and horizontal PFCs (orange cables) are not uniformly arranged, toroidally not very axisymmetric and they seem to have a general negative offset in the vertical coordinate. In addition, there is no exact knowledge of how the internal vertical coils have moved during the years, and these uncertainties presented relevant difficulties while attempting to adjust a numerical, physics-based ISTTOK model. This motivates the need for the model identification procedure discussed in section V-B.

III. ISTTOK HARDWARE

The implementation of ISTTOK's real-time control diagnostics and actuators relies on a recently upgraded hardware based on the Advanced Telecommunications Computing Architecture (ATCA). The real-time control system is programmed on top of the Multi-threaded Application Real-Time executor (MARTe) software framework [16], which collects and processes the information gathered by all the diagnostics [17]. A recently implemented, hardware-integrated, magnetic probes signals acquisition system allowed the implementation of new real-time algorithms for an accurate reconstruction of the current centroid position on ISTTOK.

A. ATCA-MIMO-ISOL BOARDS

The ATCA carrier board is an IPFN-developed board [18] complying with the ATCA standard specification, highly modularized, and with an optional Rear Transition Module (RTM) for extended connectivity. The carrier board can hold up to 32 analog input channels, each connected to a plugged-in ADC module. All modules are connected digitally to a XILINX Virtex-4 FPGA, which performs the necessary digital signal processing and includes a PCI Express Endpoint providing the data interface to the ATCA switch board. The latest version of the ATCA-MIMO-ISOL boards built at IPFN were initially developed for the magnetic acquisition in the stellarator W7-X [19], and they were then tested for use in the ISTTOK device. A picture of the ATCA board is shown in figure 7.

The phase modulated (chopper) ADC module [18] was designed targeting the digital integration of signals generated by magnetic coils, over periods of time larger than one

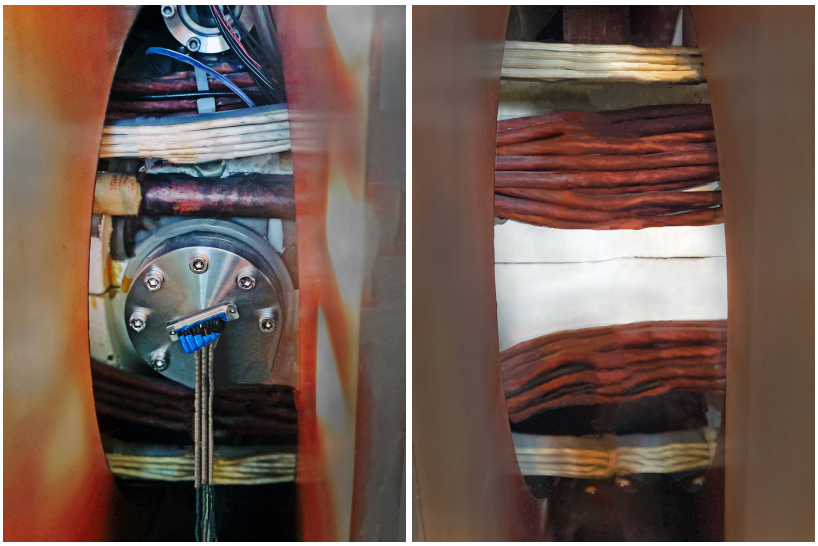

(a) Magnetic probes, which are connected to the ATCA acquisition boards. In addition, the PFCs and copper shell are also visible in the image.

(b) Close-up of the PFCs, with the white cables corresponding to the primary coils, and the orange cables representing the vertical and horizontal coils.

FIGURE 4. ISTTOK close up side views.

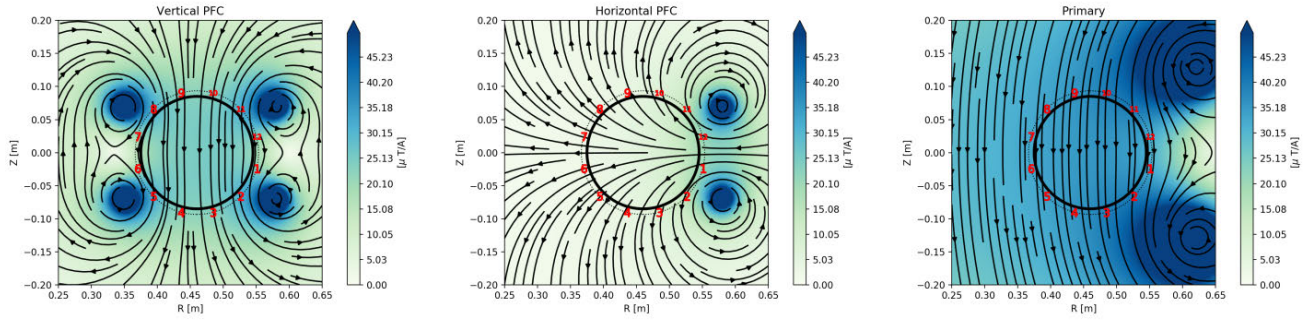

FIGURE 5. Magnetic field generated by the active coil circuits on their nominal positions. Mirnov coils are represented by their sequential numbers (in red) over the dashed line. The black circle represents the limiter.

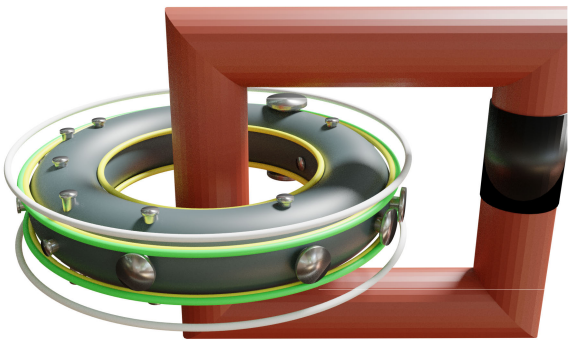

FIGURE 6. 3D model of the ISTTOK PFCs, vacuum chamber with ports, iron core and the former central solenoid (black color). Primary coils (white color) and horizontal coils (green color) are formed by 2 coils each, and are located on the upper and lower LFS (Low Field Side) of tokamak. Vertical coils (yellow color) are formed by 4 coils, 2 are located on the upper and lower LFS and 2 in the upper and lower HFS (High Field Side).

hour. This ADC module is composed by a Signal Condition block with a passive filter attenuator and an active differential amplifier, the ADC block (18-bit resolution, fixed 2MSPS (Mega samples per second)), a DC-DC converter and a galvanic isolation coupler (ILS711-S1) and finally the digital interface to the FPGA in the ATCA carrier Board. The FPGA also provides the clock signals for the DC-DC converter, the chopper and ADC clocks and receives the serial ADC data and clock signals.

IV. REAL-TIME INTEGRATION SOFTWARE

To recover the magnetic field magnitude from inductive probe signals, an integrating component is needed. However, typical electronic integrator circuits always suffer from voltage offsets present in the components and wiring. Even very low offsets integrated over a long period of time may appear as a noticeable drift of the integrated signals [20] and eventually saturate their outputs. The solution chosen for this integrator design, previously demonstrated in a four channel prototype in PXI format [19], was to modulate signals with a phase invertor (chopper), which reverses periodically the input signal before active amplification (multiplies the signal by 1 and

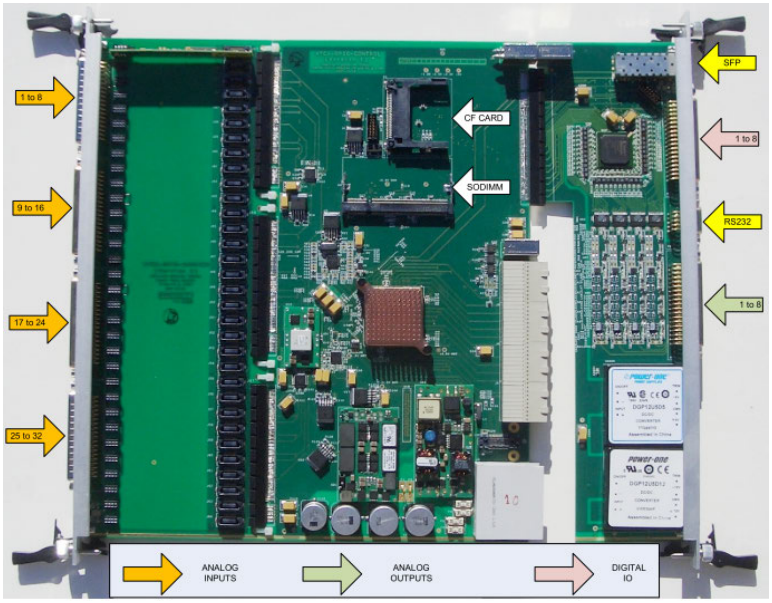

FIGURE 7. General view of the ATCA-MIMO-ISOL carrier board, including on the right side an original IPFN RTM board joined through an edge connector.

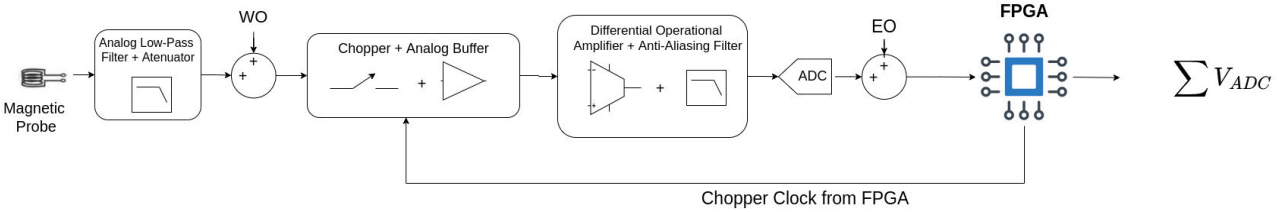

FIGURE 8. ADC module diagram depicting the influence of the WO and EO offsets and the instrumentation since the magnetic probes signal it is acquired until its integration in the FPGA.

then by -1), filtering and sampling in the ADC, as shown in figure 8. The switching frequency is programmable and made synchronous with the sampling ADC 2Mhz clock, as both are generated in the same FPGA. By applying the signal inversion before any electronic amplification, and reconstructing the digital equivalent of the signal after the digitalization, the average of the Electronics Offset (EO, i.e. the voltage offset introduced downstream of the chopper converter due to chopper charge transfers and the amplification of the ADC input, see fig. 8) is expected to be almost zero in the integration process if its value is steady enough over at least two inversion periods. In addition, a second offset also appears before the chopper, i.e. the Wiring Offset (WO) which may be generated upstream of the DC-DC converter either inside the module or in the external wiring, connectors and soldered parts, mainly due to uncompensated thermocouple effects, external interference or radiation effects (see again fig. 8). Unfortunately, the WO is not averaged by the chopping method, since it goes across two signal reversions, and is typically much lower than either both EO or the ADC resolution. From figure 8 the integration process can be inferred. If the upcoming signal from the probe is denoted by $s(t)$, the sampled value $V_{ADC}[n]$ is:

$$V_{ADC}[n] = (s(nT_s) + \mathrm{WO}) \cdot \mathrm{Ph}_{chop}(nTs) \; + \; \mathrm{EO}\,, \qquad (1)$$

where $t = nT_s$, T_s is the ADC sampling period, and Ph_{chop} is the phase signal of the chopper (1 or -1). Assuming $s(nT_s) \approx n[T]$ and $\mathrm{Ph}_{chop}(nT_s) \approx \mathrm{Ph}_{chop}[n]$, the phase reconstructed signal from the magnetic probe can thus be approximated from the discrete samples as:

$$s[n] \; \approx (V_{ADC} - \mathrm{EO}) \cdot \mathrm{Ph}_{chop}[n] - \mathrm{WO}\;. \qquad (2)$$

Assuming the ADC sampling frequency is sufficiently high with respect to the double of the the signal bandwidth, the integral of the magnetic fluxes picked up by the Mirnov coils can be approximated by the expression

$$\Phi(t = nT_s) = \int_0^{t=nT_s} s(t)dt \approx \sum_0^N ((V_{ADC}[n] - \mathrm{EO}) \cdot \; \mathrm{Ph}_{chop}[n]) - nT_s \cdot \mathrm{WO}. \qquad (3)$$

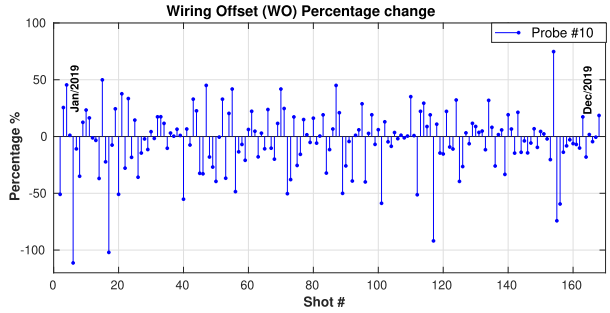

FIGURE 9. WO percentage change in the magnetic probe # 10 in 2019 using data from approximately 180 shots distributed during the entire year.

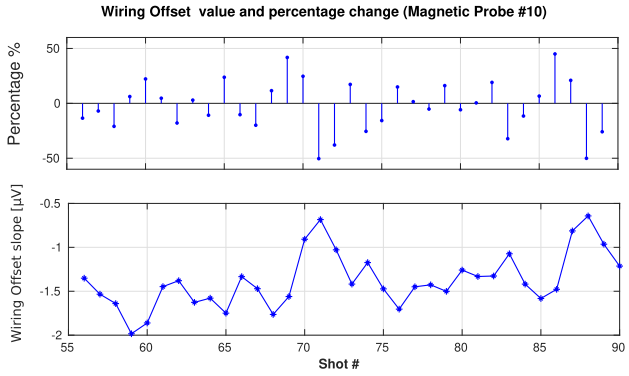

FIGURE 10. WO and percentage change in the magnetic probe #4 throughout 45 shots in ISTTOK.

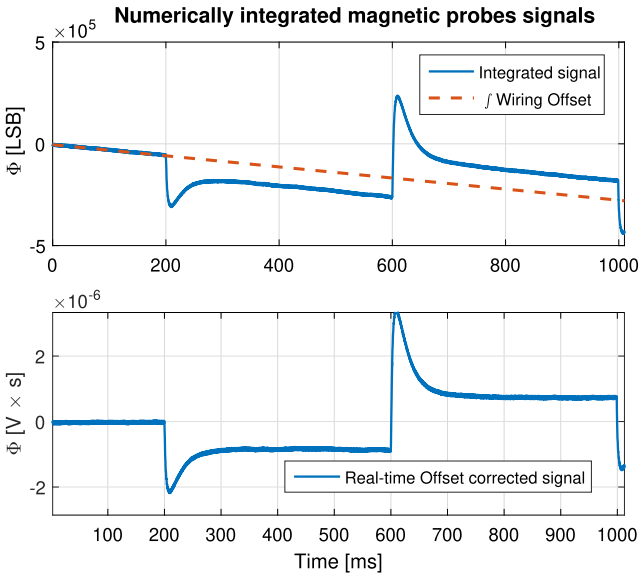

FIGURE 11. Real-time subtraction of the integrated WO for drift compensation is performed on every MARTe cycle throughout the shot and for each magnetic probe.

Hence, to approximate the integral of the signals acquired from the magnetic diagnostics, the EO-corrected V_{ADC} summation is computed in the FPGA and then sent to the MARTe database via PCI-express.

Even though WO removal is a common feature in processing magnetic data, the solution implemented at ISTTOK gives a remarkable flexibility in allowing the calculation of the offset prior to each discharge. This is in contrast with other experiments, where the offset correction is fixed and calibrated one sigle time. Due to the physical conditions in ISTTOK, which do not include a good isolation of the instrumentation for minimizing electromagnetic noise and temperature impact, the offset drift values are in constant change and so they should be calculated prior to every discharge. Figure 9 shows the WO fluctuation in the magnetic probe # 10 in 2019, it is possible to see that in most of the shots the changing percentage is in the order of $\pm$ 30%. Figure 10 shows the WO values and percentage changes for a less number of shots on the magnetic probe #10, this shot numbers correspond to data acquisitions where the WO had the smallest changes, from these figures is possible to conclude that a real-time algorithm is needed to calculate the WO on each probe prior to a plasma discharge.

Even though the probes signals are not stored in the experiment database before the start of discharge, the WO of each probe can be computed several seconds prior to the beginning of the discharge. The obtained WO value is then subtracted in real-time at every MARTe iteration from the actual probe signals once the discharge starts. In figure 11, the integrated WO summed to the probe signal is shown.

V. ISTTOK REAL-TIME PLASMA POSITION CONTROL

The real-time measurements of the plasma current and centroid position are used in the implementation of a feedback control loop for these quantities. The reconstruction of these quantities has been widely addressed in the previous work presented in [14]. The controller design, on the other hand, is based on a state-space model that links the PF currents to the quantities of interest; such model is obtained through a data-driven procedure, discussed in section V-B.

In practice, the control of the plasma current centroid position is then achieved by means of several programming blocks working together, also known in MARTe as General Application Modules (GAMs). A block diagram of the control loop architecture is shown in figure 12. The control cycle starts with the acquisition of the signals from the magnetic probes. These signals are processed in the ''Magnetics'' GAM, where the radial and vertical centroid position are computed for every MARTe cycle. Then, the ''Controller'' GAM selects the controller to be used for the centroid position based on the data selected in the ''Discharge Configurator'' GUI, which is configured by the tokamak operator before the start of the discharge; the control inputs are computed either by the ''PID'' (Proportional-Integral-Derivative) GAM or the ''LQR'' (Linear-Quadratic Regulator) GAM, discussed later in this section. These inputs are sent back to the ''Controller'' GAM, which provides them as control signals to the PFCs power supplies.

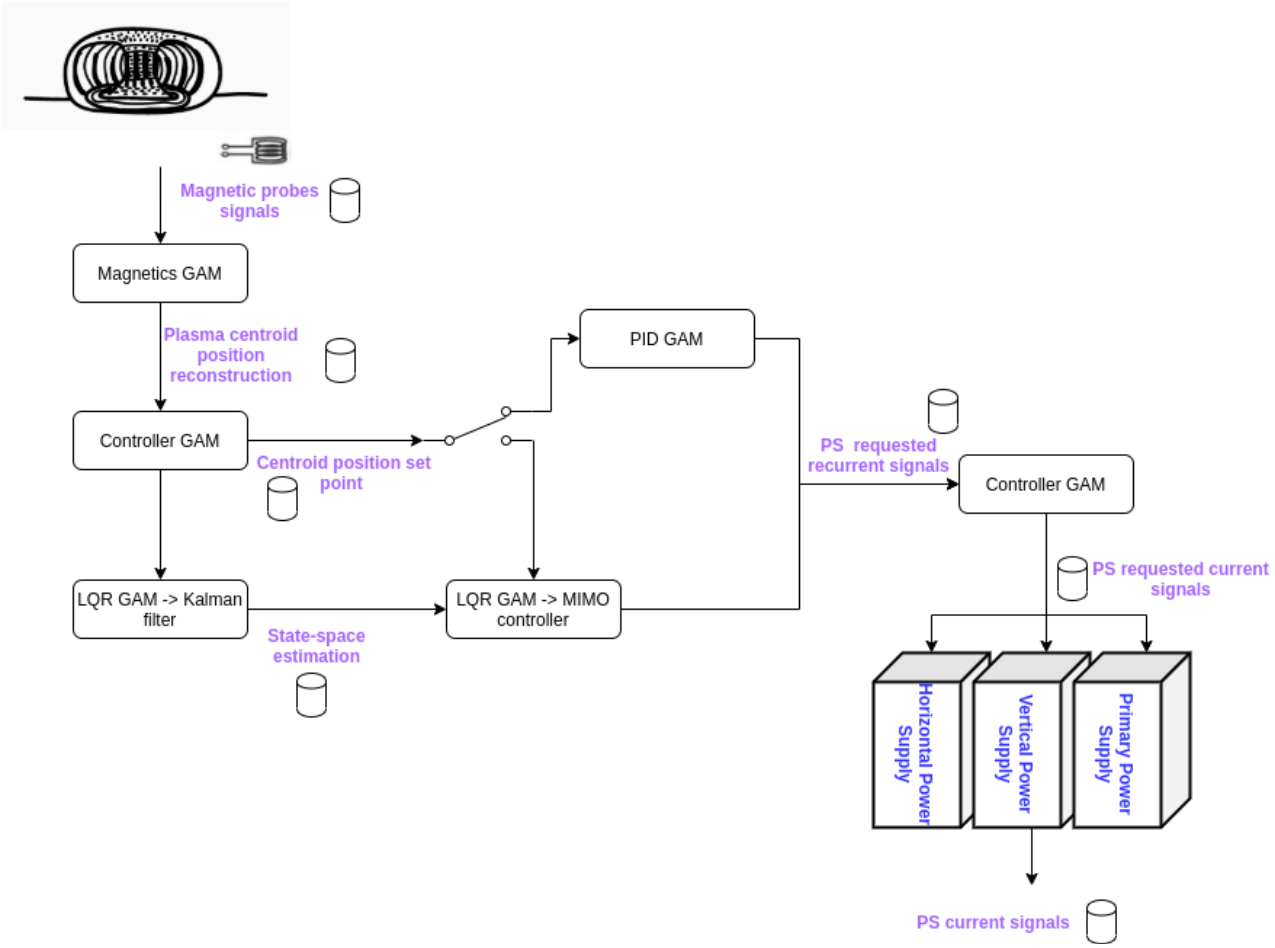

FIGURE 12. ISTTOK MARTe overal plasma position control scheme.

Since the ISTTOK tokamak is operated in AC mode, during the transition from negative to positive (or opposite) plasma current the reconstruction of the centroid position is inhibited, as it gives non-valid results. During the transitions, which last $\sim$ 1ms, a pre-programmed, open-loop configuration of the PFCs currents is used, which means that there is a constant switching from automatic to manual control in between plasma cycles. The switching process between controllers may produce jumps at the plant inputs: this is known as the *bumpless transfer* problem [21, Chapter 8]. To minimize these jumps, the control signal at the manual-to-automatic switching instant should be made as close as possible to the value it assumed during manual mode [22].

A. PID CONTROL IMPLEMENTATION

Early tokamaks often employed sets of PFCs that were symmetrically placed with respect to the tokamak equatorial plane, in order to guarantee mutually independent vertical and horizontal movement of the plasma [3, Chapter 1]. For many years, ISTTOK plasma position control strategy was driven by the principle that an external vertical field generates an horizontal force and an horizontal external field generates a vertical force due to the Lorentz force law. This in turn led to the implementation of two separate SISO (Single-Input Single-Output) controllers for the vertical and radial centroid position. The "PID" GAM in figure 12 implements the same algorithm in the MARTe framework: it has two PID controllers with pre-configured gains, an anti-windup system[1] and a bumpless transfer mechanism, obtained by adjusting the integral action when the saturation limits are reached and/or when the transition from manual to automatic control takes place [24, Chapter 3], [22].

B. DATA-DRIVEN STATE-SPACE MODEL RETRIEVING

This original SISO logic has been upgraded to a MIMO one, which relies on a data-driven model of the plasma behaviour This model is discussed in this section.

As it was discussed in section II-C, obtaining an accurate physics-based electromagnetic model (either axisymmetrical

[1]The saturation of actuators or major set point changes are some of the most frequent non-linearities in control applications, which can cause instabilities in the system. The undesired interplay of these events with the integral action of a PID controller is called *windup* [23]. It typically produces undesired overshoots resulting from overreaction of the integrator block of a PID controller [21, Chapter 1], and must hence be compensated for.

or 3D) for the ISTTOK plasma response is a hard task, due to the large uncertainties in the machine geometry and parameters. Early efforts in finding a theoretical model for ISTTOK magnetic control were performed during the last years. However, since ISTTOK PFCs are not axially symmetric and apparently their actual positions have shifted from the original ones, despite the efforts a working theoretical model was never successfully obtained. For this reason, finding an alternative path to implement a model-based magnetic control in the ISTTOK real-time MARTe system became necessary. In particular, in order to design the plasma position controller, data-driven models of the plasma response were obtained from past discharges data by means of Matlab's *System Identification Toolbox* [25]. These models are in the form of 2×2 MIMO systems, with the Vertical and Horizontal PF circuits currents as inputs and the vertical and radial plasma current centroid coordinates as outputs. In practice, 10 state variables were found to be enough in order to achieve a sufficiently accurate description of the centroid position dynamics. It is worth to remark that, in general, models based on first principles often employ the currents flowing in the active circuits, in the plasma and in the machine passive structures as state variables. The currents in the active circuits, in particular, can be either regarded as states (and the corresponding applied voltages are used as control inputs) or as input variables (in which case they are considered as impressed currents and removed from the state vector). For the identified models used in this work, the input and output vectors are defined as $u^T = [I_{vert}, I_{hor}]$ and $y^T = [R, z]$ respectively. However, in this case the state variables obtained through the identification procedure do not have a straightforward physical interpretation.

When trying to join data sets of signals coming from positive and negative plasma current discharges, the models started to loose consistency, showing from early stages that the two discharge phases needed to be modeled separately. Hence, one state-space model was obtained for discharges where $I_p > 0$, and another for discharges where $I_p < 0$. This matter probably originates from the fact that a tokamak is not completely axisymmetric in reality. This is particularly true for ISTTOK, which happens to have very non-axisymmetric PFCs that can produce a different overall topology of the poloidal magnetic field in the tokamak for the $I_p > 0$ and $I_p < 0$ cases. Figures 13 and 14 show the comparison between the database centroid position signals and their reconstruction using the estimated state-space models. It is worth to remark that these are validation plots, i.e. the reconstructed centroid position was not used as modeling data. Differences in the transients of the signals might originate from differences in the initial states between systems.

Since a tokamak is an intrinsically nonlinear system, the modeling process was done using data sets in which the centroid position was located in a prescribed region, in order to approximate the estimated model to an equilibrium region where a linear approximation is valid. Local linearized models are typically evaluated in a set of operating points that capture the key modes of operation. Linear controllers like PID or LQR are then synthesized for the obtained linear system, ensuring that some relevant performance specifications are met in the vicinity of the operating point in question [26].

C. KALMAN FILTER IMPLEMENTATION

In order to reconstruct the state vector x, two Kalman filters were also implemented, one for the model related to positive plasma current and another for the negative current one. The Kalman filter matrices were chosen based on noise estimates obtained from ISTTOK experimental data, calculating the co-variance matrices from the signal vectors [27]. Figures 15b and 15a correspond to the real-time Kalman filter reconstruction of the vertical and radial plasma centroid position and its comparison with the multi-filament reconstructed position computed by the "Magnetics" GAM.

D. MULTIPLE-INPUT MULTIPLE-OUTPUT CONTROL IMPLEMENTATION

The full-state estimate from the Kalman filter is generally used in conjunction with the full-state feedback control law from LQR, resulting in the optimal, sensor-based linear-quadratic Gaussian (LQG) controller [28, Chapter 8]. Under this principle, the real-time reconstructed states are multiplied by the control LQR gain K in order to steer the vertical and radial plasma centroid position towards a desired set point; this process is computed in the "LQR" GAM. The weight matrices for the discrete LQR controller were empirically tuned in order to have a balance between a fast response and the input energy demand. In particular, for the examples proposed in this article, a discrete-time LQR implementation has been used. The considered infinite-horizon cost function is given by

$$J = \sum_{n=0}^{\infty} x^T(n) Q x(n) + u^T(n) R u(n)\,,$$

where the weighing matrices have been tuned empirically and chosen as

$$Q = \mathrm{diag}(10, 1500, 1, 10, 10, 1, 1, 2, 0.01, 10)$$
$$R = \mathrm{diag}(0.07, 3 \cdot 10^{-5})$$

for the case with positive I_p and

$$Q = \mathrm{diag}(800, 0.1, 0.01, 0.01, 0.01, 10, 10, 0.1, 0.01, 0.01)$$
$$R = \mathrm{diag}(5 \cdot 10^{-3}, 7 \cdot 10^{-3})$$

for the case with negative I_p. However, several algorithms for a non-empirical calculation of the LQR matrices exist, some of which propose a tuning based on experimental data with a gain matrix that can be iteratively updated [29, Chapter 9], [30].

VI. PLASMA CURRENT CENTROID POSITION CONTROL RESULTS

In the following plots, the control performance in terms of vertical and horizontal plasma centroid coordinates is

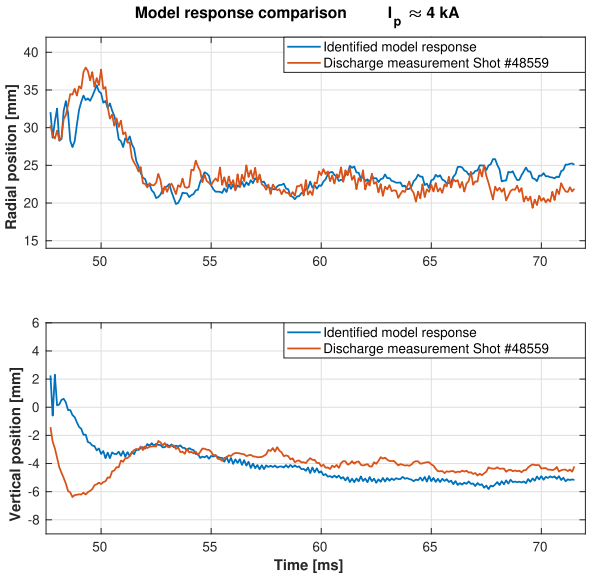

(a) Comparison between the identified model response and the real-time centroid position reconstruction. Shot #48559

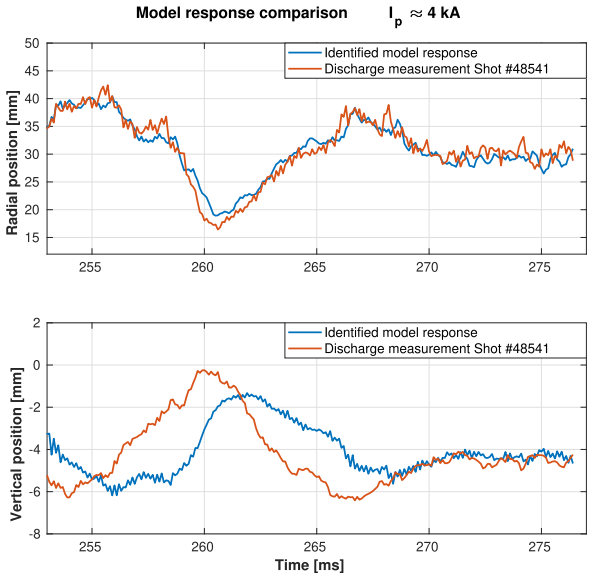

(b) Comparison between the identified model response and the real-time centroid position reconstruction. Shot #48541

FIGURE 13. Model response for two different $I_p \approx 4$ kA discharges.

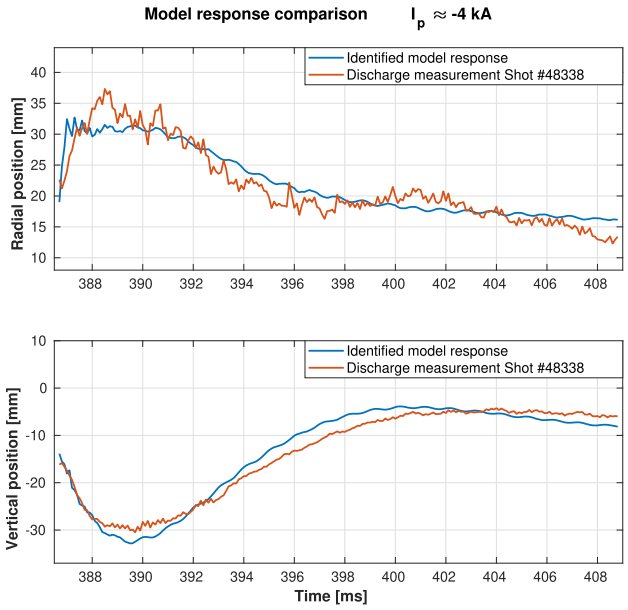

(a) Comparison between the identified model response and the real-time centroid position reconstruction. Shot #48338

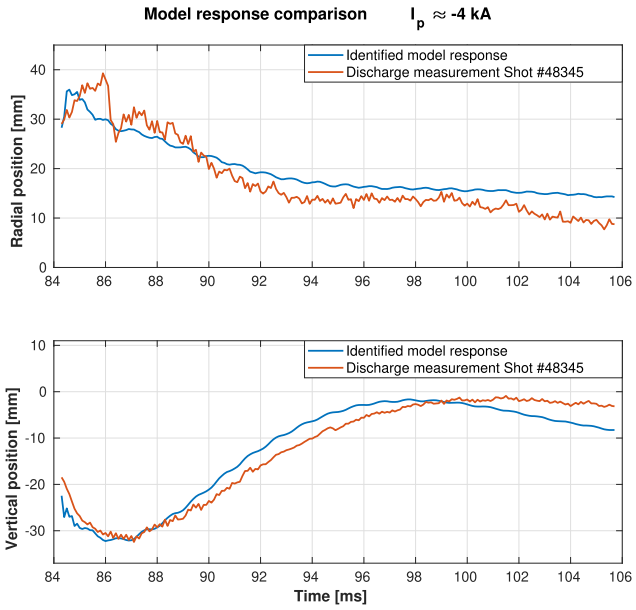

(b) Comparison between the identified model response and the real-time centroid position reconstruction. Shot #48345

FIGURE 14. Model response for two $I_p \approx -4$ kA discharges.

compared for the cases where these quantities are controlled by a set of 2 PID's and by a single LQR MIMO controller, and for different pre-programmed set points. The resulting control inputs, i.e. the vertical and horizontal PFCs currents, are also shown and compared in the considered cases. In the figures, the discharges are referred to as *Shot#* followed by the ISTTOK's database discharge number. Since it is not mathematically possible to determine the initial conditions of the states, they must be steered to the MIMO controller region of attraction. This is achieved by controlling the centroid

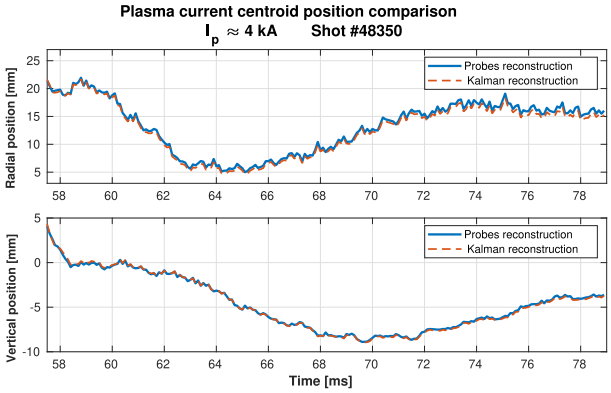

(a) Real-time Kalman filter retrieved centroid position compared against the multi-filament reconstruction time trace for $I_p > 0$.

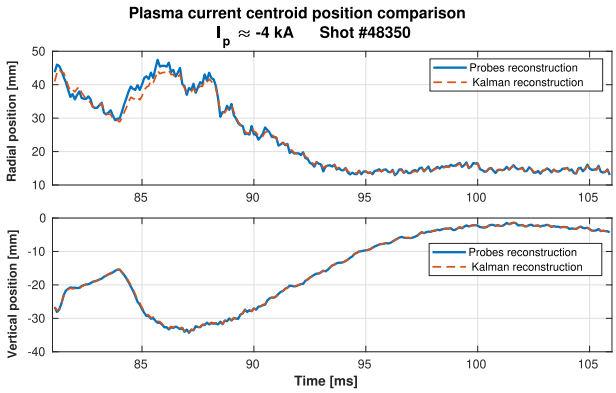

(b) Real-time Kalman filter retrieved centroid position compared against the multi-filament reconstruction time trace for $I_p < 0$

FIGURE 15. **Comparison of the Kalman-filtered centroid position with the multi-filament reconstruction.**

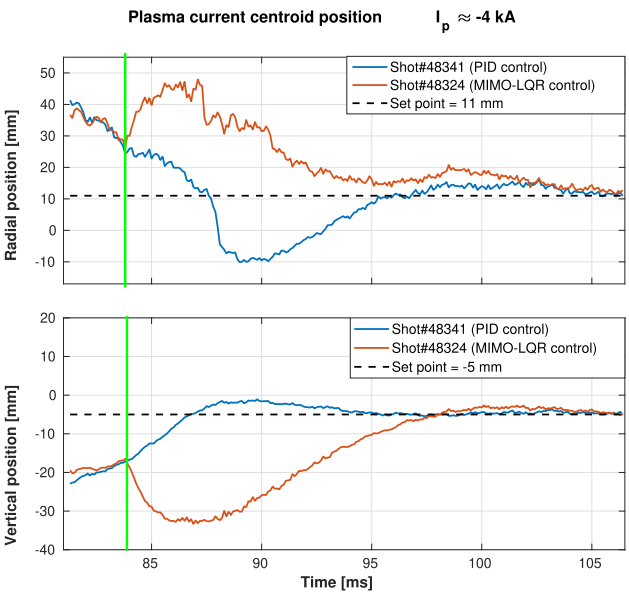

(a) $I_p \approx 4$ kA. Blue time trace corresponds to a PID feedback control and orange time trace to a LQR feedback control, the dashed black line shows the programmed set point. The green vertical line marks the time instant at which the discharge Shot#48324 switches from PID to LQR control.

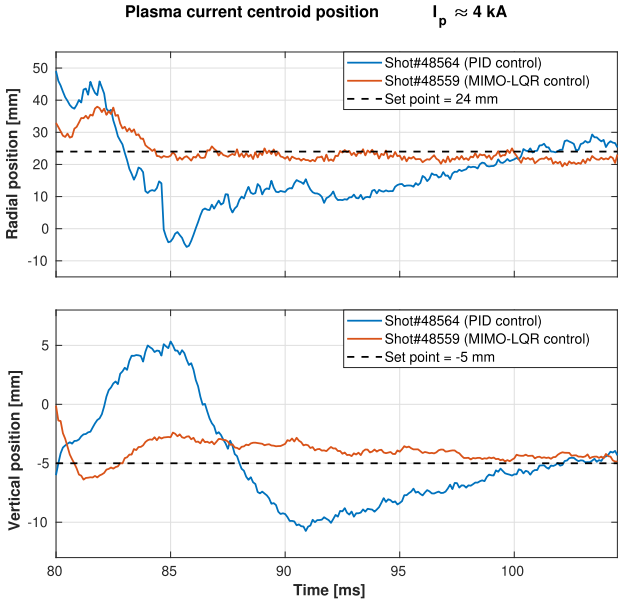

(b) $I_p \approx 4$ kA . Blue time trace corresponds to a PID feedback control and orange time trace to a LQR feedback control, the dashed black line shows the programmed set point.

FIGURE 16. **Horizontal and vertical plasma centroid positions.**

position with the PIDs at the beginning of the discharge, while the Kalman filter converges to the actual value of the state vector. For this reason, the discharges marked as LQG control start with PID controllers and then switch to LQG at $t \sim 1$ *ms* for positive I_p plasmas and at $t \sim 3.5$ *ms* for negative I_p ones (the switching instants can be configured by the user). Switching between two controllers in parallel yields a control substitution which causes bumps in the response; bumpless transfer schemes can be modified in order to smooth the phasing-in of a new controller to supplement or replace an existing control at the plant, e.g. as described in [26].

Figures 16a and 16b show the time traces of the vertical and horizontal plasma centroid position for two different scenarios. Figure 16a shows the plots corresponding to a plasma discharge where $I_p \approx -4$ kA; the green vertical line marks the switching point from PID to LQG control. The vertical position time trace shows a non-minimum phase system behavior for the MIMO LQG control, while this behaviour is absent for the PID case. It is possible that this behavior origins from a delay that was introduced as a numerical artifact during the data-driven identification process.[2] Figure 16b corresponds to a plasma discharge where $I_p \approx 4$ kA; since the

[2]Open-loop and closed-loop models for $I_p \approx -4$ kA have a zero far from the unitary circumference in the transfer function $H_2(z)$ map which links the vertical centroid position z and the vertical PFCs current I_{vert}; this might have generated an initial undershoot in the vertical centroid position response.

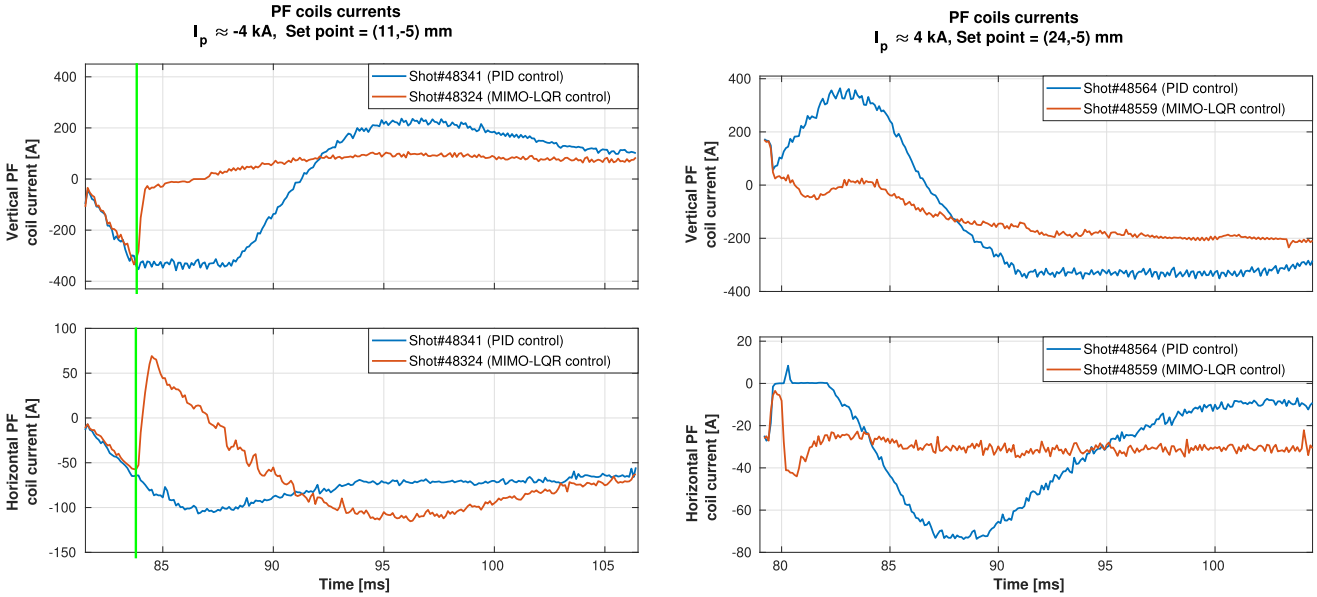

(a) $I_p \approx -4$ kA. Blue time trace corresponds to a PID feedback control and orange time trace to a LQR feedback control. The green vertical line marks the time when the discharge Shot#48324 switches the control from PID to LQR.

(b) $I_p \approx 4$ kA. Blue time trace corresponds to a PID feedback control and orange time trace to a LQR feedback control.

FIGURE 17. Vertical and Horizontal PFCs currents.

PID controlled part of the discharge is very short in this case, the switching point is not marked. The position set points are shown as black dashed lines in both figures.

Figure 16 indicates that the LQG controller has significantly improved performance when Ip is positive. However, in the case of a negative Ip, the LQG controller's performance is comparable to the PIDs on the radial position channel, although with a slightly shorter settling time. Instead, it is slower than the PIDs on the vertical position channel but both attain the setpoint with practically no error in a reasonably short time.

As shown in fig. 17, for the case with positive I_p a noticeably smaller current request from the vertical and horizontal PFCs power supplies can be appreciated in the LQG case, which implies less power is required by the system with the updated controller. The resulting input currents are smaller with respect to the ones requested by the PID controller also for the vertical position channel in the case with $Ip \approx -4$ kA, while in this case comparable input signals can be observed on the radial position channel.

VII. CONCLUSION

This article provides a comprehensive account of the recent advancements made to the plasma current centroid position control system of the ISTTOK tokamak. In addition to describing the new and improved hardware and software components used to implement this control system, the article also delves into the technical details and specifications of these components. By providing a detailed account of the control system's architecture, the article aims to provide insights into the underlying principles and mechanisms of the ISTTOK plasma centroid position control. An *ad-hoc* offset compensation mechanism has been implemented to take into account the AC plasma current in the ISTTOK device, and a data-driven model identification was performed in order to identify the plasma centroid position response to variations in the PF currents. A novel MIMO LQG controller was designed and tested, and a comparison with the results obtained resorting to the pre-existing PID control logic shows that comparable or better performance can be obtained with a reduced energy consumption from the PFCs power supplies.

ACKNOWLEDGMENT

Views and opinions expressed are however those of the author(s) only and do not necessarily reflect those of the European Union or the European Commission. Neither the European Union nor the European Commission can be held responsible for them.

REFERENCES

[1] J. Wesson and D. J. Campbell, *Tokamaks*, vol. 149. Oxford, U.K.: Oxford Univ. Press, 2011.

[2] M. L. Walker, P. De Vries, F. Felici, and E. Schuster, "Introduction to tokamak plasma control," in *Proc. Amer. Control Conf. (ACC)*, Jul. 2020, pp. 2901–2918.

[3] A. Pironti and M. Ariola, *Magnetic Control of Tokamak Plasma*. Cham, Switzerland: Springer, 2016.

[4] G. Ambrosino and R. Albanese, "Magnetic control of plasma current, position, and shape in Tokamaks: A survey or modeling and control approaches," *IEEE Control Syst. Mag.*, vol. 25, no. 5, pp. 76–92, Oct. 2005.

[5] A. Pironti and M. Walker, "Fusion, tokamaks, and plasma control: An introduction and tutorial," *IEEE Control Syst.*, vol. 25, no. 5, pp. 30–43, Oct. 2005.
[6] G. De Tommasi, R. Albanese, G. Ambrosino, M. Ariola, P. J. Lomas, A. Pironti, F. Sartori, and J.-E. Contributors, "Current, position, and shape control in tokamaks," *Fusion Sci. Technol.*, vol. 59, no. 3, pp. 486–498, Apr. 2011.
[7] M. L. Walker and D. A. Humphreys, "On feedback stabilization of the tokamak plasma vertical instability," *Automatica*, vol. 45, no. 3, pp. 665–674, Mar. 2009.
[8] G. De Tommasi, A. Mele, Z. P. Luo, A. Pironti, and B. J. Xiao, "On plasma vertical stabilization at EAST tokamak," in *Proc. IEEE Conf. Control Technol. Appl. (CCTA)*, Aug. 2017, pp. 511–516.
[9] L. L. Lao, H. St. John, R. D. Stambaugh, A. G. Kellman, and W. Pfeiffer, "Reconstruction of current profile parameters and plasma shapes in tokamaks," *Nucl. Fusion*, vol. 25, no. 11, pp. 1611–1622, Nov. 1985.
[10] D. Abate, M. Bonotto, and P. Bettini, "Sensitivity analysis of low-order plasma moments reconstruction for RFX-mod2 tokamak operations," *Fusion Eng. Des.*, vol. 182, Sep. 2022, Art. no. 113243.
[11] Y. Huang, Z. P. Luo, B. J. Xiao, L. L. Lao, A. Mele, A. Pironti, M. Mattei, G. Ambrosino, Q. P. Yuan, Y. H. Wang, and N. N. Bao, "GPU-optimized fast plasma equilibrium reconstruction in fine grids for real-time control and data analysis," *Nucl. Fusion*, vol. 60, no. 7, Jul. 2020, Art. no. 076023.
[12] C. Varandas et al., "Engineering aspects of the tokamak ISTTOK," *Fusion Technol.*, vol. 29, no. 1, pp. 105–115, 1996.
[13] T. Guerra, "Real-time measurement of the plasma electron density at ISTTOK," M.S. thesis, Universidade Tecnica de Lisboa, Lisbon, Portugal, Tech. Rep. 395137798647, 2008. [Online]. Available: https://fenix.tecnico.ulisboa.pt/downloadFile/395137798647/dissertacao.pdf
[14] D. Corona, A. Torres, E. Aymerich, A. Cianciulli, A. D. Falco, B. B. Carvalho, H. Figueredo, H. Alves, and H. Fernandes, "Extraction of the plasma current contribution from the numerically integrated magnetic signals in ISTTOK," *J. Instrum.*, vol. 15, no. 2, Feb. 2020, Art. no. C02020.
[15] I. S. Carvalho, P. Duarte, H. Fernandes, D. F. Valcárcel, P. J. Carvalho, C. Silva, A. S. Duarte, A. Neto, J. Sousa, A. J. N. Batista, T. Hekkert, and B. B. Carvalho, "ISTTOK real-time architecture," *Fusion Eng. Des.*, vol. 89, no. 3, pp. 195–203, Mar. 2014.
[16] A. C. Neto, F. Sartori, F. Piccolo, R. Vitelli, G. De Tommasi, L. Zabeo, A. Barbalace, H. Fernandes, D. F. Valcarcel, and A. J. N. Batista, "MARTe: A multiplatform real-time framework," *IEEE Trans. Nucl. Sci.*, vol. 57, no. 2, pp. 479–486, Apr. 2010.
[17] I. S. Carvalho, P. Duarte, H. Fernandes, D. F. Valcárcel, P. J. Carvalho, C. Silva, A. S. Duarte, A. Neto, J. Sousa, A. J. N. Batista, and B. B. Carvalho, "ISTTOK control system upgrade," *Fusion Eng. Des.*, vol. 88, nos. 6–8, pp. 1122–1126, Oct. 2013.
[18] A. J. N. Batista, A. Neto, M. Correia, A. M. Fernandes, B. B. Carvalho, J. C. Fortunato, J. Sousa, C. A. F. Varandas, F. Sartori, and M. Jennison, "ATCA control system hardware for the plasma vertical stabilization in the JET tokamak," *IEEE Trans. Nucl. Sci.*, vol. 57, no. 2, pp. 583–588, Apr. 2010.
[19] M. Werner, A. Endler, J. Geiger, and R. Koenig, "W7-X magnetic diagnostics: Rogowski coil performance for very long pulses," *Rev. Sci. Instrum.*, vol. 79, no. 10, pp. 1–5, 2008.
[20] P. Spuig, P. Defrasne, G. Martin, M. Moreau, P. Moreau, and F. Saint-Laurent, "An analog integrator for thousand second long pulses in tore supra," *Fusion Eng. Des.*, vols. 66–68, pp. 953–957, Sep. 2003.
[21] P. Hippe, *Windup in Control Its Effects and Their Prevention*. Cham, Switzerland: Springer, 2011. [Online]. Available: http://www.springer.com/engineering/control/book/978-0-85729-634-4
[22] Y. Peng, D. Vrančić, and R. Hanus, "Anti-windup, bumpless, and conditioned transfer techniques for PID controllers," *IEEE Control Syst.*, vol. 16, no. 4, pp. 48–57, Aug. 1996.
[23] P. Hippe, *Windup in Control: Its Effects and Their Prevention*. Cham, Switzerland: Springer, 2006.
[24] H. Yu, T. Xie, and B. Wilamowski, "Recent advances in industrial control," in *Proc. Ind. Electron. Conf. (IECON)*, 2011, pp. 4626–4631, doi: 10.1109/IECON.2011.6120073.
[25] I. The MathWorks. *System Identification Toolbox*. Natick, MA, USA. Accessed: May 15, 2023. [Online]. Available: https://www.mathworks.com/help/ident/
[26] J. D. Bendtsen, J. Stoustrup, and K. Trangbaek, "Bumpless transfer between observer-based gain scheduled controllers," *Int. J. Control*, vol. 78, no. 7, pp. 491–504, May 2005.
[27] A. Mele, G. De Tommasi, A. Pironti, and B. J. Xiao, "Shape reconstruction and eddy currents estimation via Kalman filter at the EAST tokamak," in *Proc. 45th EPS Conf. Plasma Phys.*, Jul. 2018, pp. 417–420.
[28] S. L. Brunton and J. N. Kutz, *Data-Driven Science and Engineering: Machine Learning, Dynamicl Systems, and Control*. Cambridge, U.K.: Cambridge Univ. Press, 2019.
[29] F. Franklin, *Digital Control of Synamic Systems*, 3rd ed. Half Moon Bay, CA, USA: Ellis-Kagle Press, 1998.
[30] S. Trimpe, A. Millane, S. Doessegger, and R. D'Andrea, "A self-tuning LQR approach demonstrated on an inverted pendulum," in *Proc. 19th World Congr. Int. Fed. Autom. Control*, 2014, vol. 19, no. 3, pp. 11281–11287.

DOMÉNICA CORONA received the joint Ph.D. degree from the Advanced Program in Plasma Science and Engineering, Universidade de Lisboa, and UniversitÃ degli Studi di Padova, in 2021. She is currently an Associate Researcher with the Princeton Plasma Physics Laboratory, Computer Sciences Department, NJ, USA. Her current research interests include real-time magnetic control, machine learning, and data-driven approaches for Tokamak models and active control.

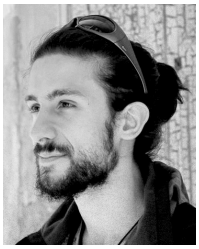

ADRIANO MELE received the M.Sc. degree (Hons.) in automation engineering from the University of Naples Federico II, in 2015, and the joint Ph.D. degree in nuclear fusion science and engineering from the University of Naples and the University of Padua, in 2019. He has been a Visiting Researcher with EAST Tokamak, Hefei, China, the Swiss Plasma Center of EPFL, Lausanne, Switzerland, the ITER Remote Experimentation Center, Rokkasho, Japan, and the Princeton Plasma Physics Laboratory, Princeton, NJ, USA. He was a recipient of the EuroFusion Engineering Grant dedicated to the development of diagnostic systems for the forthcoming DTT Tokamak and an Adjunct Professor in information technology for industrial automation with the University of Napoli Federico II. He is currently a Researcher with the University of Tuscia, Viterbo, Italy. His research interests include control engineering, in particular with applications to fusion plasmas, including the investigation of data-driven and machine learning methods.

NUNO CRUZ has focused on diagnostics and control algorithm development and control and data acquisition systems integration for several fusion devices, including JET, ITER, Tokamakã configuration variable (TCV), and JT-60SA. His current research interests include the design and development of high performance software and algorithms for the ITER radial neutron camera, algorithms for edgelocalized mode mitigation using vertical plasma kicks in TCV, optimal control for plasma vertical stabilization for TCV, and magnetic control tools for JT-60SA.

HUGO ALVES received the degree in engineering physics from Instituto Superior Tecnico, Lisbon, Portugal, in 2011. From 2014 to 2020, he was an ISTTOK Operator and was in charge of technical maintenance, such as vacuum systems, gas injection, data acquisition, diagnostics, power electronics, and fast amplifiers along with the development of FPGA firmware and linux device driver development for control and data acquisition on the COMPASS (Prague, Czech Republic) and Wendelstein 7-X (Greifswald, Germany) fusion experiments.

BERNARDO B. CARVALHO received the Ph.D. degree in physics engineering from Instituto Superior Técnico, Lisbon, Portugal, in 2003. He was a Chief Engineer with the European Shock-Tube for High Enthalpy Research Laboratory, Instituto Superior Técnico. He coordinates the control and data acquisition (CODAC) systems on the ISTTOK Tokamak. His current research interests include CODAC for fusion devices, including electronic instrumentation, field-programmable gate array data processing, magnetic probes, and MHD diagnostics.

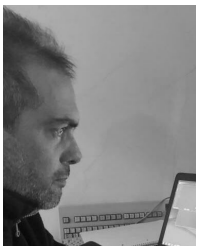

HUMBERTO FIGUEIREDO received the M.Sc. degree in engineering physics from Instituto Superior Técnico, Lisbon, Portugal, in 2000. Since 2000, he has been holding the position of an Engineer in charge with ISTTOK Tokamak, where he is responsible for overseeing its technical maintenance and operation. He has also been involved in various research projects related to plasma physics, including the study of plasma turbulence, plasma instabilities, and the behavior of plasma under extreme conditions.

HORACIO FERNANDES received the Graduate degree in engineering physics and the Ph.D. and Habilitation degrees from ULisboa. He is currently a Professor with Instituto Superior Técnico, ULisboa. He is also a Senior Researcher with Instituto de Plasmas e Fusão Nuclear, where he is a member of the BoD, acts as the Chair of the Experimental Group and the Director of the IST-TOK Tokamak. He had taught several courses in the university, covering general physics, electronic instrumentations, and plasma physics, and has been a supervisor of more than 25 master's students and seven Ph.D. students. Since 1999, he has been developing a remote controlled laboratory presently hosting more than 20 experiments on-line some of them dispersed all over the world. Related to that, he taught courses for high school teachers. He is a member of the Portuguese Physics Society and has been a treasurer. He is also a member of IUPAP's Commission on Physics for Development and the Chairs of the General Assembly of the Physics Union of Portuguese-speaking countries. He had a role in a few international institutions (e.g., a scientific investigator in a CRP-IAEA project, a fusion for energy member of the technical advisor panel, and a SC member of the fusion-DC Erasmus mundus). At IST, he had served in several administrative boards, such as the President of the Post-graduate Students Union, a member of the University General Assembly, the Vice President of the Physics Department, and the Faculty Deputy Director.